FLI1 and GATA1 govern *TLN1* transcription: new insights into FLI1-related platelet disorders

Elisa Gabinaud,[1] Laurent Hannouche,[1] Mathilde Veneziano-Broccia,[1] Johannes Van Agthoven,[2] Justine Suffit,[1] Julien Maurizio,[1] Delphine Potier,[3] Dominique Payet-Bornet,[3] Delphine Bastelica,[1] Elisa Andersen,[1] Manal Ibrahim-Kosta,[1] Timothée Bigot,[1] Céline Falaise,[4] Hemostasis Unit of Lille,[5] Anne Vincenot,[6] Pierre-Emmanuel Morange,[1] Paul Saultier,[1,4] Marie-Christine Alessi[1,4] and Marjorie Poggi[1]

[1]Aix-Marseille Univ, INSERM, INRAe, C2VN, Marseille, France; [2]Structural Biology Program, Division of Nephrology/Department of Medicine, Massachusetts General Hospital and Harvard Medical School, Charlestown, MA, USA; [3]Aix-Marseille Univ, CNRS, INSERM, Institut Paoli-Calmettes, CRCM, Marseille, France; [4]APHM, CHU Timone, French Reference Center on Inherited Platelet Disorders, Marseille, France; [5]Hemostasis Unit, Hospital University Center Lille, Lille, France and [6]CHU Robert Debré, National Reference Center for Inherited Platelet Disorders and Biological Hematology Service, AP-HP, Paris, France

Correspondence: M. Poggi
marjorie.poggi@univ-amu.fr

Received: August 1, 2024.
Accepted: December 16, 2024.
Early view: January 2, 2025.

https://doi.org/10.3324/haematol.2024.286372

Abstract

Germline variants of FLI1, essential for megakaryopoiesis, are linked to bleeding disorders, platelet aggregation defects and mild thrombocytopenia. However, the mechanisms behind these abnormalities remain unclear. This study aims to elucidate the impact of FLI1 variants on human megakaryocytes and platelets. We focused on four FLI1 variants, two of which are novel: p.G307R and p.R340C. We assessed the impact of FLI1 variants on megakaryopoiesis using single-cell RNA sequencing, and defects were confirmed in patients' platelets and cell lines. Results showed variants p.R337Q, p.K345E and p.R340C exhibited faulty nuclear localization and defective transcriptional activity *in vitro* and variants p.K345E and p.G307R affected protein stability. A total of 626 genes were differentially expressed in patient megakaryocytes, including genes associated with the platelet activation pathway. *TLN1* was among the most down-regulated genes, with an 88% reduction in talin-1 protein levels in FLI1 patients' platelets. Analysis of chromatin immunoprecipitation sequencing data revealed FLI1-binding regions in the *TLN1* gene. Luciferase reporter gene assays revealed the functional role of an intronic binding region in cooperation with GATA1. FLI1 variants were linked to reduced cooperative transcriptional activity. These findings reveal novel mechanisms underlying the pathogenicity of FLI1 variants. Defective cooperation between FLI1 variants and GATA1 may play a role in talin-1 deficiency in FLI1 patients' platelets, thus contributing to platelet dysfunction. Moreover, talin-1 could serve as a biomarker for classifying the pathogenicity of FLI1 variants.

Introduction

FLI1 belongs to the Ets gene family encoding transcription factors that share a conserved DNA-binding domain known as the ETS domain, which recognizes specific DNA sequences (GGA(A/T)). FLI1 plays a critical role in vasculogenesis, angiogenesis, and megakaryocytic differentiation. FLI1 can either repress or activate the expression of various megakaryocyte (MK)-specific genes by cooperating with partner transcription factors.[1-3] Mice with a targeted null *FLI1* variation die at day 11.5 of embryogenesis due to loss of vascular integrity, resulting in bleeding within the vascular plexus of the cerebral meninges.[4] Additionally, mice lacking the carboxy-terminal regulatory domain of FLI1 exhibit thrombocytopenia as well as defective platelet activation and aggregation.[5]

The role that FLI1 plays in platelet production and function in humans was initially elucidated in patients with Paris-Trousseau syndrome, who exhibit a deletion at chromosome 11q23, which includes the *FLI1* gene.[6] Germline defects in FLI1 that disrupt its transcriptional activity were documented two decades later.[7-9] These defects cause the rare constitutional bleeding disorder platelet-type 21 (BDPLT21) as listed in the Online Mendelian Inheritance in Man database. Similar to patients with an 11q23 deletion, carriers of FLI1 variants show reduced MK ploidy and size, a decrease in platelet dense granules, enlarged and fused alpha granules, and an impaired aggregation response to platelet agonists.[9] However, the effects of *FLI1* variations on FLI1 protein and megakaryopoiesis are not fully understood.

In this study, we characterized two new FLI1 variants. Transcriptome analysis of CD34⁺-derived MK revealed that *TLN1* is a direct target of both FLI1 and GATA1, highlighting the crucial cooperation between these two transcription factors, which is disrupted in some FLI1 variants.

Methods

The methods concerning single-cell RNA sequencing (scRNA-seq) analysis, platelet phenotyping, cell culture conditions, luciferase reporter assay, Western blot assay, epifluorescence microscopy, protein stability assay, structural model of FLI1 interactions, fibrinogen binding to platelets, electrophoretic mobility shift assay (EMSA) and proximity ligation assay are described in the *Online Supplementary Appendix*.

Patients and DNA sequencing

Genetic analyses were conducted at the French Reference Center for Inherited Platelet Disorders (CRPP) at La Timone University Hospital in Marseille, France. All cases were included in the study after obtaining written informed consent in accordance with protocols approved by national institutional review boards and the principles of the Declaration of Helsinki (authorization number 20200T2-02). Four FLI1 variants were evaluated in this study; two of them, p.R337Q and p.K345E (NM_002017.3, c.1009C>T and c.1033A>G, respectively), have already been reported by our team. The two additional variants p.G307R and p.R340C (NM_002017.3, c.919G>A and c.1018C>T, respectively) were discovered through sequencing of the gene panel dedicated to hereditary platelet disorders and implemented by the CRPP.

CD34⁺-derived megakaryocyte culture and scRNA-seq

CD34⁺-derived megakaryocyte culture and scRNA-sequencing were conducted as previously described.[10] After density gradient separation (Eurobio), circulating CD34⁺ cells were purified using positive selection with magnetic beads (MiltenyiBiotec) and then cultured in StemSpan Serum-Free Expansion Medium II supplemented with Megakaryocyte Expansion Supplement (STEMCELL Technologies). CD34⁺-differentiated cells from 2 healthy individuals and patient A2 harboring the FLI1 R337Q variant were harvested from cultures on days 5 and 11. Cell concentrations and viability were assessed after trypan blue staining with an automated cell counter (Eve™ NanoEntek). The cell samples from each individual were labeled with a distinct hashtag oligo (TotalSeq-C, Biolegend) and pooled. Single-cell isolation was then carried out with the 10x Genomics Technology using the Chromium Next GEM Single Cell 5'Kit v2 (ref 1000263), according to the manufacturer's protocol. Single cell complementary DNA synthesis and sequencing libraries were prepared with a single-cell 5' Library and Gel Bead kit (10x Genomics Technology). Libraries were sequenced using a 75-bp paired-end reads format with Next-seq500 (GBiM platform) (parameters, read 1: 26 cycles, i7: 8 cycles, read 2: 57 cycles).

Statistical analysis

Quantitative variables are expressed as the mean ± standard error. Analyses were performed using GraphPad Prism software. Statistical differences were determined via Kruskal-Wallis or Mann Whitney tests as indicated in the figure legends. $P<0.05$ was considered statistically significant.

Results

Patients' characteristics

Five patients were analyzed; their clinical characteristics are provided in Table 1. The characteristics of affected members from families A and B have been previously documented.[9] Since the previous publication, patient A2 had recurrent episodes of diffuse bilateral pulmonary hemorrhaging from 2018 to 2021, requiring hospitalization and red blood cell (RBC) transfusions. Extensive testing did not identify a clear cause other than a platelet defect. Analysis of platelets from patients A1, A2, and B showed a defect in dense granules and reduced platelet aggregation

Table 1. Clinical characteristics of patients carrying the FLI1 variants.

Case	DNA change	AA change	Gender	Age*	Clinical features
A1	c.1010G>A	p.R337Q	Male	54	Spontaneous ecchymosis
A2	c.1010G>A	p.R337Q	Male	27	Gingivorrhagia, three episodes of lung hemorrhages
B	c.1033A>G	p.K345E	Female	60	Hematomas, epistaxis, menorrhagia, RBC transfusion during delivery and epistaxis
C	c.1018C>T	p.R340C	Male	10	Ecchymosis, prolonged bleeding from cuts, epistaxis
D	c.919G>A	p.G307R	Female	44	Ecchymosis, menorrhagia, bleeding after avulsion of wisdom teeth, abortion and delivery requiring RBC transfusion

*Age (in years) at the time of the last evaluation. AA: amino acid; RBC: red blood cell.

in response to collagen, adenosine diphosphate (ADP) and thrombin receptor-activating peptide 6 (TRAP6). Patients A2 and B had mild thrombocytopenia.[9]

The proband of families C and D, ages 10 and 44 years, respectively, harbored novel FLI1 variants. The child of family C presented with prolonged bleeding, purpura, and epistaxis, and a bicuspid aortic valve with dilation of the ascending aorta. Platelet tests revealed reduced CD63 expression in response to TRAP6 and low mepacrine uptake, serotonin and ADP levels consistent with a diagnostic of storage pool disease (*Online Supplementary Table S1*). Electron microscopy showed large alpha granules (*Online Supplementary Figure S1*). Platelet testing showed reduced aggregation responses to ADP and collagen. The 44-year-old proband from family D was assessed for moderate thrombocytopenia (86-147x10^9/L) and significant bleeding episodes, including menorrhagia and postpartum hemorrhaging. Extraction of her third molars was complicated by bleeding. Surgical correction of interventricular communication required RBC transfusions. Platelet analysis revealed no platelet aggregation defects. Blood smear analysis showed giant alpha granules in several platelets (*Online Supplementary Figure S1*). She exhibited decreased platelet serotonin levels and undetectable ATP release after TRAP6 stimulation, suggesting storage pool disease (*Online Supplementary Table S2*).

Characterization of two novel FLI1 variants

The two newly identified FLI1 variants, G307R and R340C, were characterized and compared with the previously described variants, R337Q and K345E.[9] All mutations are located in the ETS DNA-binding domain (Figure 1A). We examined the transcriptional activity of the variants using a dual-luciferase reporter assay. Co-transfection of the reporter plasmid containing the ETS-binding sites and the plasmid encoding wild-type (WT) *FLI1* in MSR cells (GripTite293 macrophage scavenger receptor cell line) resulted in a 70% decrease in luciferase activity. Replacing WT *FLI1* with any of the *FLI1* variants, except the G307R variant, led to a significant decrease in repressive activity (Figure 1B). Western blot analysis showed that the levels of mutant FLI1 proteins exhibiting reduced activity *in vitro* were comparable to those of WT FLI1 (Figure 1C). As previously described for the R337Q and K345E variants, the biomarker MYH10 was over-expressed in the platelets of patients carrying R340C and G307R variants, while the protein was barely detected in control samples, thus confirming the pathogenicity of both novel variants (Figure 1D).

Fluorescence microscopy showed that WT FLI1 and FLI1 G307R were concentrated primarily in cell nuclei, whereas the other FLI1 variants were predominantly located in the cytoplasm (Figure 1E), thereby suggesting that the G307R variant has a distinct pathogenic mechanism. Concordant with the fluorescence microscopy results, subcellular fractionation showed increased FLI1 protein levels in the cytoplasmic fraction and decreased levels of FLI1 in the nuclear fraction in MSR cells expressing the R337Q, K345E and R340C variants compared with cells expressing WT FLI1 or the G307R variant (*Online Supplementary Figure S2*).

Reduced protein stability of FLI1 variants

We assessed protein stability using cycloheximide (CHX), an inhibitor of eukaryotic translation. FLI1 protein levels were measured at different time points after CHX treatment, which are expressed as a percentage of the initial FLI1 protein levels (0 hours of CHX treatment) and normalized to GAPDH expression levels (Figure 1F). The G307R and K345E mutations led to an approximately 60% decrease in the half-life of the mutant proteins.

Structural analysis of the FLI1-DNA interaction and FLI1 homodimers

A structural analysis shed light on the deleterious effect of each mutation. In the X-ray structure of the FLI1 DNA binding domain in complex with double stranded DNA[11] residues R337, R340 and K345 are located at the DNA/FLI1 interface (Figure 2A). Specifically, R337 and R340 form hydrogen bonds with guanine bases 5 and 4, respectively (Figure 2A, Inset A), while K345 salt-bridges the phosphate backbone (Figure 2A, Inset B). Using the SAMPDI-3D web server,[12] we calculated positive ΔΔG values for R337Q, R340C and K345E. While R337Q nearly reaches the critical 1 kcal/mol value (0.98 kcal/mol), R340C and K345E are clearly categorized as disruptive at 1.49 and 1.48 kcal/mol, respectively (*Online Supplementary Table S3*). In contrast, G307 is distant from the DNA/FLI1 interface and has a negligible impact on protein-DNA binding (Figure 2A and *Online Supplementary Table S3*).

Additionally, we assessed the structural aspects of FLI1 homodimerization. In the FLI1 homodimer R337, R340 and K345 are away from the homodimer interface (Figure 2B). Furthermore, low ΔΔG values of FLI1 homodimerization upon mutations R337Q, R340C, and K345E, obtained through the Mutabind2 web server,[13] predicted a minimal effect. The G307R mutation, however, located at the core of the homodimer interface near the contact residue N306 (Figure 2B, Inset A) showed a substantial ΔΔG value of 3.59 kcal/mol (*Online Supplementary Table S4*) potentially impeding dimerization through steric hindrance and charge repulsion.

Aberrant megakaryocyte populations in FLI1 variant cells

To investigate the impact of FLI1 variants on megakaryopoiesis, we conducted scRNA-seq on circulating $CD34^+$ cells differentiated into MK *in vitro* and analyzed at culture days 5 and 11. The cells were derived from healthy controls and a patient carrying the R337Q mutation. We used UMAP (Uniform Manifold Approximation and Projection) dimensional reduction to visualize cell transcriptome heterogeneity. Using unsupervised clustering and lineage signature gene sets, cell types were assigned as previously described.[10]

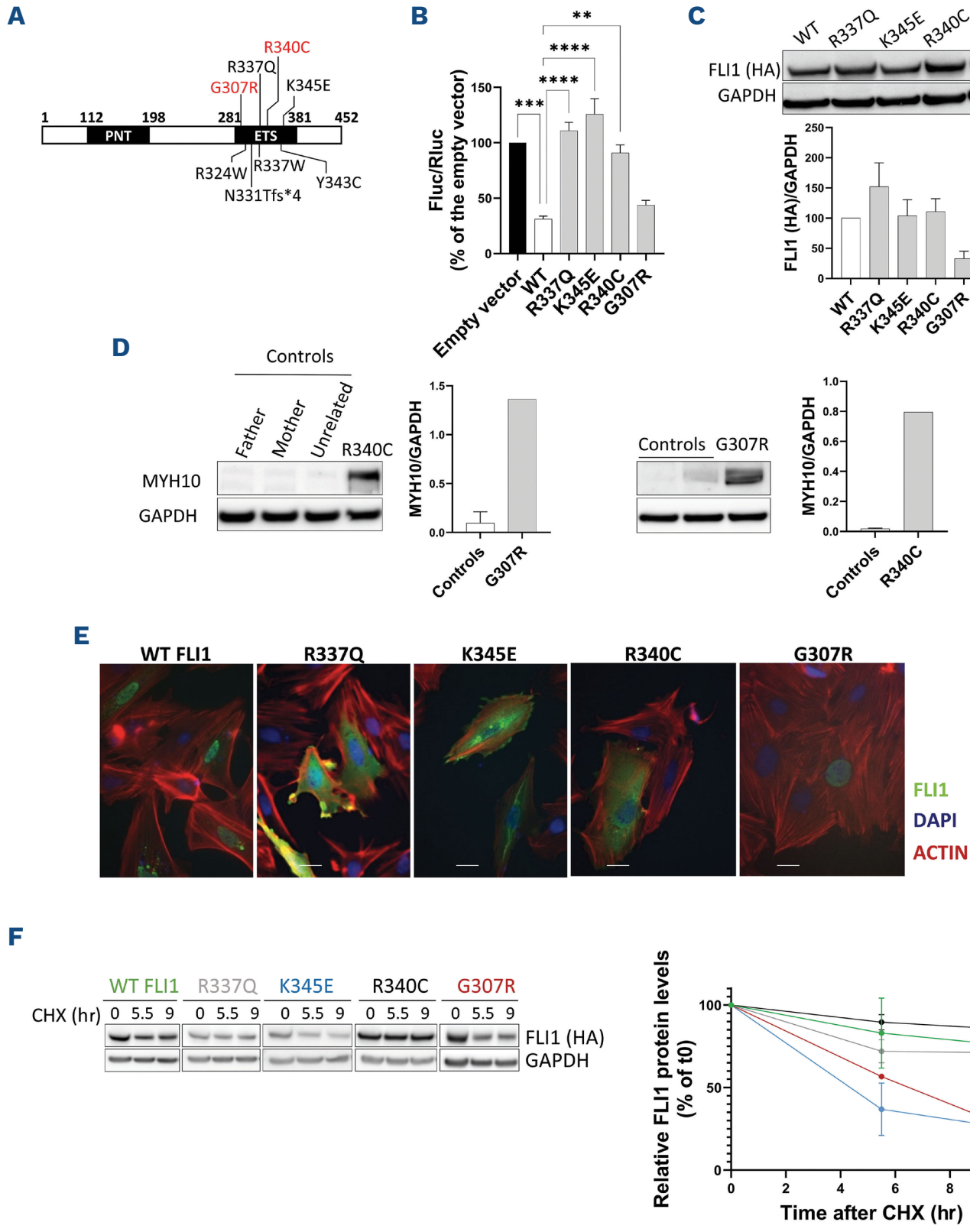

Figure 1. Functional characterization of the two novel FLI1 variants. (A) Schematic diagram of the FLI1 protein. The functional N-terminal Pointed (PNT) and C-terminal ETS (ETS) DNA-binding domains are depicted. The position of the variations in FLI1 is indicated in red (new variations described in this study) or black (previously reported variations). (B) MSR cells were co-transfected with an empty vector, wild-type (WT) *FLI1* or *FLI1* variant constructs, including the previously reported FLI1 variants,[9] along with the Firefly luciferase reporter plasmid containing three tandem copies of the ETS-binding site upstream of the HSV TK promoter (E743tk80Luc) and the pGL4.73 Renilla luciferase control vector. The Firefly to Renilla luminescence ratios (Fluc/Rluc) were calculated to normalize for transfection efficiency and are expressed as percentage relative to the empty vector. Data represent mean ± standard error of the mean (SEM) of ten independent experiments; ***P*<0.01, ****P*<0.001, *****P*<0.0001 *versus* WT (Kruskal-Wallis test). (C) Representative Western blot analysis of FLI1 expression in MSR cells transfected with WT *FLI1* or *FLI1* variant constructs. We verified FLI1 expression using an anti-HA antibody. GAPDH was used as a protein loading control. (Bottom) Results of the densitometric analysis are expressed as mean ± SEM. Three independent experiments were performed. (D) Representative Western blot analysis of MYH10 expression in washed platelets from FLI1 variant carriers. R340C was compared to two unaffected family members (father and mother) and one unrelated control. G307R was compared to two unrelated controls. GAPDH was used as a protein loading control. (Right) Densitometric analysis results were normalized to GAPDH and expressed as mean ± SEM. (E) Representative immunofluorescence microscopy images of H9C2 cells transfected with WT *FLI1* or *FLI1* variant constructs visualized using immunofluorescence after FLI1 (anti-HA antibody), nucleus (DAPI) and ACTIN (rhodamine phalloidin) staining; scale bar, 5 μm. (F) Effect of FLI1 variations on the half-life of FLI1 protein. MSR cells were transfected with WT *FLI1* or *FLI1* variant constructs. After 48 hours (hr), cells were treated with cycloheximide (CHX) for the indicated times (0, 5.5 or 9 hr). Cells were lysed, and cell lysates were then subjected to Western blot analysis. (Right) Densitometric analysis results are expressed as mean ± SEM. FLI1 levels at each time point are represented relative to the initial levels at time zero (t0). Two independent experiments were performed.

We identified the major hematopoietic cell stages: hematopoietic stem/progenitor cells (HSPC), common myeloid progenitors (CMP), granulocyte-monocyte progenitors (GMP), MK-erythroid progenitors (MEP), and progenitor and mature MK (MKP-MK) (Figure 3A).

In early cell stages (HSPC, CMP and GMP), the transcriptome profiles of control and patient cells were highly similar. However, distinctive gene expression patterns were observed as early as the MEP stage, which was more pronounced at the MKP/MK stage. Together with the increased FLI1 expression levels in MK (Figure 3B), these observations indicate that FLI1 plays an important role in MK maturation. Furthermore, the number of differentially expressed genes (DEG) between control and patient cells increased over the course of cell differentiation, especially at the MEP and MK stages (*Online Supplementary Figure S3*). Erythroid-related genes are among the top 20 genes showing increased expression in patient MEP (*HBG2, HBB, GYPB*, and *BLVRB*) and MKP/MK (*HBE1, HBG2, HBB, GYPB, BLVR*B, and *KLF1*) (*Online Supplementary Figure S4*). KLF1 was the most up-regulated regulon (comprising TF and their targets) in FLI1-deficient MK cells, and the fifth most up-regulated in FLI1-deficient MEP cells (*Online Supplementary Figure S5*). DEG were enriched in various biological pathways in the KEGG gene set database (Figure 3C and *Online Supplementary Figure S6*). The platelet activation pathway was the most enriched pathway for down-regulated DEG in patient MK (Figure 3C), with 24 genes displaying decreased expression compared with control MKP-MK (Figure 3D). Using i-cisTarget,[14] we identified ETS binding motifs significantly over-represented in the regulatory regions of DEG in the platelet activation pathway. The canonical FLI1 motif (M07089) had a high normalized enrichment score (NES) of 5.2. Among these 24 genes, 18 have highly ranked DNA regions for the M07089 motif, indicating they are potential direct targets of FLI1. *TLN1*, one of the most down-regulated genes (fold change: 1.5, $P<0.001$), had the top-ranked FLI1-binding region (ranked first among 29 detected FLI1-binding regions) (Figure 3E).

Reduced talin-1 protein levels in FLI1 patient platelets

We confirmed the decrease in talin-1 protein levels via immunoblotting using platelet samples obtained from the 5 patients belonging to 4 different families carrying the R337Q, K345E, G307R and R340C variants, compared with age- and gender-matched healthy controls (Figure 4A). No differences were observed in other major cytoskeletal proteins, such as filamin (FlnA) or myosin heavy chain 9 (MYH9), in patients' platelets compared with healthy controls (*Online Supplementary Figure S7*). Additionally, we observed a decrease in fibrinogen binding by stimulated platelets derived from K345E and R340C variant carriers, thus indicating defective αIIbβ3 activation (Figure 4B), which cannot be attributed to a reduction in surface αIIbβ3 expression.[9]

FLI1 regulates *TLN1* transcription in cooperation with GATA1

Our findings suggest that FLI1 regulates *TLN1* expression. Silencing of endogenous FLI1 using FLI1 siRNA resulted in a decrease in talin-1 protein levels in the hematopoietic MEG-01 cell line (Figure 4C). We then acquired GATA1, RUNX1, SCL and FLI1 chromatin immunoprecipitation sequencing (ChIP-seq) data from primary human MK (deposited by the Göttgens laboratory) from the Gene Expression Omnibus (GEO) database.[15] Peak enrichments at the *TLN1* locus were extracted and visualized using the UCSC genome browser. We identified four enriched binding regions for the FLI1 transcription factor in the *TLN1* gene (Figure 5A). One of these binding regions is situated in the *TLN1* promoter

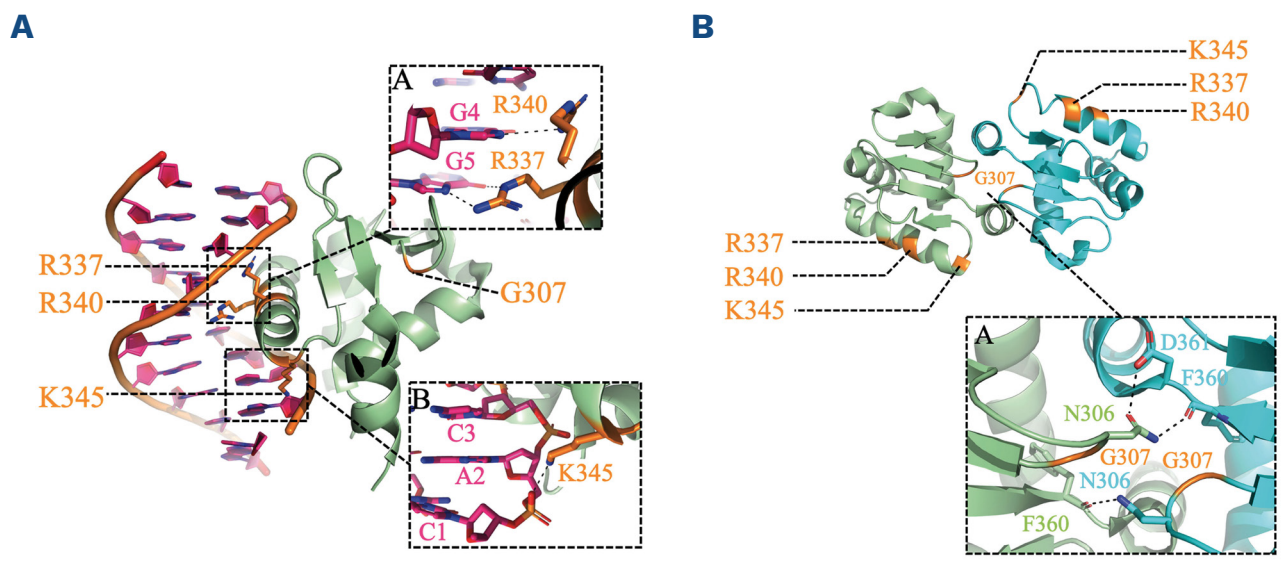

Figure 2. Structural model of FLI1 interactions. (A) Structure of FLI1 bound to double-stranded DNA (PDB: 5e8i). FLI1 shown in pale green and the double-stranded DNA in pink cartoon. FLI1 residues G307, R337, R340, and K345 are colored in orange. Nucleotides, R337, R340 (Inset A), and K345 (Inset B) are shown in sticks at the FLI1/DNA interface. Hydrogen bonds and salt bridges are depicted in black dashed lines (< 3.5Å). Oxygen atoms are in red, nitrogen in blue, and phosphorus in orange. (B) Structure of FLI1 dimer (PDB: 5e8i). FLI1 monomers 1 and 2 shown in pale green and cyan cartoon, respectively, with residues G307, R337, R340, and K345 colored in orange. Inset A shows the FLI1 1/2 dimer with residues G307 and contact residues N306, D361, and F360 in sticks. Atoms and contacts are represented as in (A).

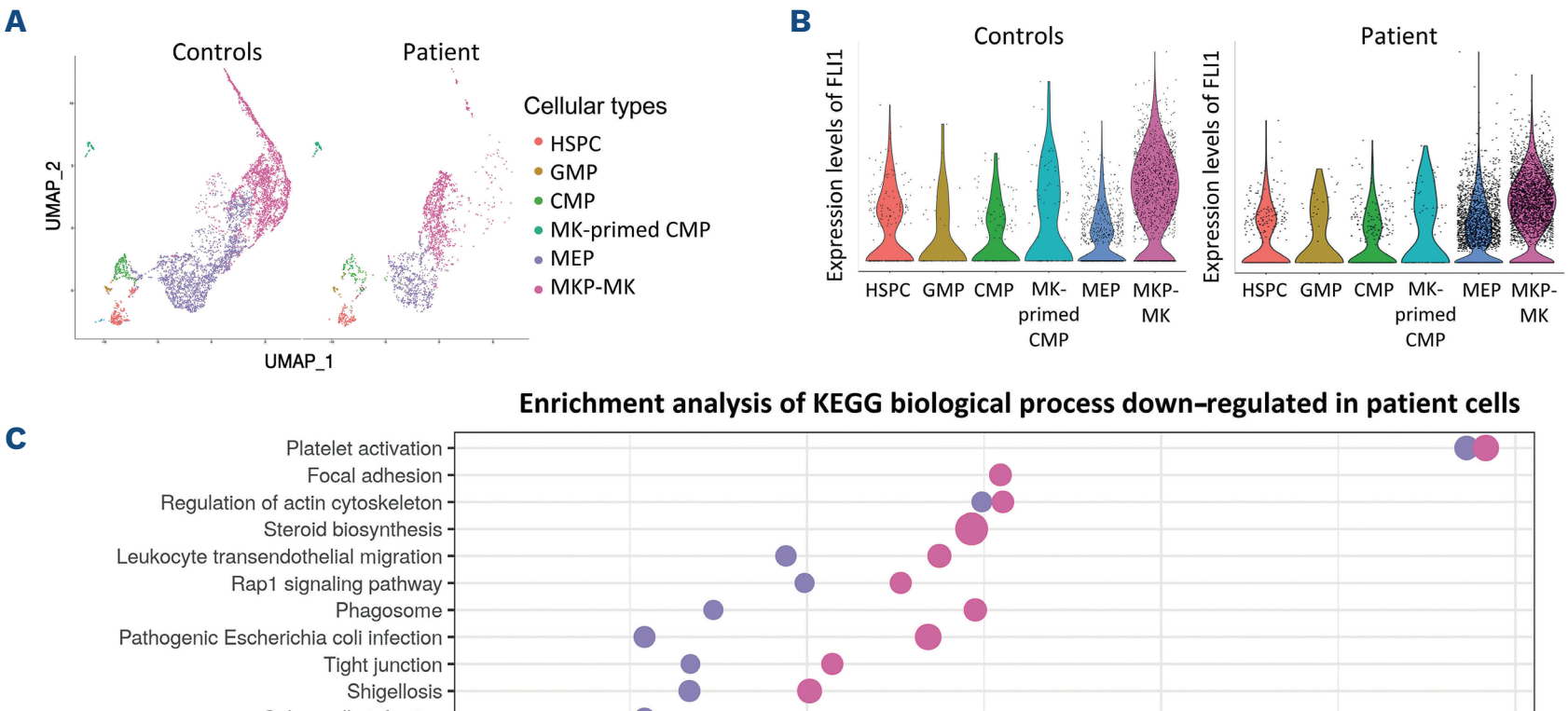

Figure 3. Single-cell RNA sequencing of cells derived from the FLI1 R337Q variant carrier and healthy controls. (A) UMAP plot of the FLI1 R337Q variant and control cells colored according to identified hematopoietic cell types: hematopoietic stem/progenitor cells (HSPC), common myeloid progenitors (CMP), megakaryocyte (MK)-primed CMP, granulocyte-monocyte progenitors (GMP), MK-erythroid progenitors (MEP), and progenitor and mature MK (MKP/MK). (B) Violin plots showing FLI1 mRNA levels in different hematopoietic cell types from healthy subjects (left) and the FLI1 patient (right). Each cell type is color-coded. (C) Bubble plot depicting the top down-regulated enriched KEGG biological pathways based on differentially expressed genes (DEG) by cell type (classified by *P* value). Dot sizes reflect the ratio of genes enriched in this pathway to the total number of genes in the pathway. Bubbles are color-coded according to cell type (HSPC, CMP, MK-primed CMP, GMP, MEP, MKP/Mk). (D) Bar plot illustrating the fold change of DEG in the platelet activation pathway, specifically of the MKP-MK cell type. (E) I-cis target results on the 24 genes of the platelet activation pathway. PWM: position weight matrix; NES: normalized enrichment score.

(chr9:35732119-35732518) (Figure 5A, indicated in purple). The other regions (chr9:35727623-35727967, chr9:35728277-35728673 and chr9:35729618-35730535, referred to as intronic binding sites 1, 2, and 3, respectively) are located in the first intron and also contained potential binding sites for RUNX1, SCL or GATA1.

To ascertain whether FLI1 regulates *TLN1* transcription through these binding regions we initially assessed the functionality of these binding regions using a luciferase reporter assay in human erythroleukemia (HEL) cells expressing hematopoietic transcription factors. (The experimental design is described in *Online Supplementary Figure S8*). Three regions (the promoter, intronic binding site 2 and intronic binding site 3) significantly increased luciferase expression, while the intronic binding site 1 region repressed luciferase expression (Figure 5B). To avoid the interference of endogenous hematopoietic transcription factors, we utilized a non-hematopoietic model, MSR cells, to identify which transcription factors bind to these regulatory regions. Based on the ChIP-seq results, we transfected transcription factors along with the putative binding sequences and evaluated luciferase activity (*Online Supplementary Figure S9*). For the promoter, binding site 1 and binding site 2 sequences, the corresponding transcription factors (i.e., FLI1, FLI1 + RUNX1, and FLI1 + GATA1, respectively) were unable to regulate luciferase transcription (*Online Supplementary Figure S9*). For binding site 3, we observed a significant increase in luciferase transcription activity due to co-transfection of FLI1 and GATA1 (Figure 5C). However, the simultaneous addition of SCL led to a decrease in luciferase activity, thus indicating that SCL exerts a repressive effect on the FLI1 and GATA1 cooperation. The three FLI1 variants R337Q, R340C and G307R abolished the synergistic transcriptional activation mediated by the FLI1 and GATA1 cooperation, which was not observed with the FLI1 K345E variant (Figure 5D). Co-overexpression of FLI1 and GATA1 in the MEG-01 cell line led to a significant increase in talin-1 protein levels (Figure 6A), which further supports the hypothesis that the FLI1 and GATA1 cooperation plays a role in regulating *TLN1* expression. Given the observed synergy in the transcriptional activation of *TLN1* intronic binding site 3 by FLI1 and GATA1, we performed an EMSA analysis to determine whether FLI1 and GATA1 bind to the *TLN1* intronic binding site 3 region. When *TLN1* intronic binding site 3 was incubated with nuclear proteins extracted from cells transfected with FLI1 or GATA1, specific retarded

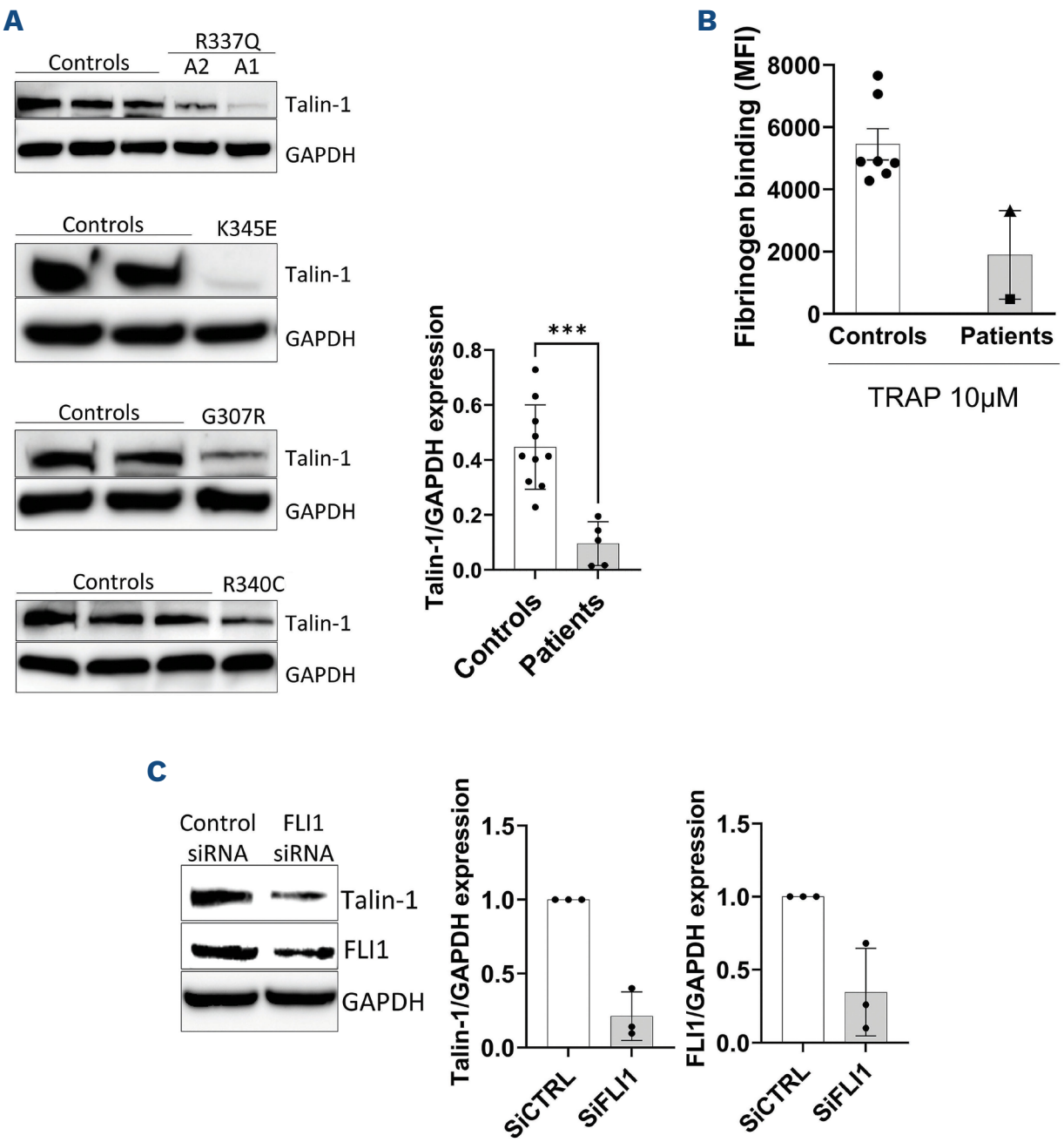

Figure 4. Talin-1 levels and fibrinogen binding in FLI1-deficient cells. (A) Western blot analysis of talin-1 expression in washed platelets from controls and FLI1 variant carriers. GAPDH was used as a protein loading control. Each patient was compared with age- and sex-matched control subjects. For each patient and matched controls, blood samples were collected at the same time and processed in parallel to avoid any bias. Quantification of band intensity is shown on the right. ***P<0.001 (Mann-Whitney test). (B) Binding of labeled fibrinogen (Fibrinogen-FITC) to washed platelets from controls and FLI1 variant carriers (K345E■ and R340C▲) upon activation with 10 µM TRAP6 for 15 minutes. Fibrinogen binding fold change values represent the mean fluorescent intensity (MFI) of fibrinogen bound by stimulated platelets, subtracted from the MFI under resting conditions. (C) FLI1 siRNA were transfected into MEG-01 cells. Endogenous FLI1 and talin-1 expression levels were quantified via Western blot analysis (N=3 per group). GAPDH was used as a protein loading control. (Right) Band intensity was quantified.

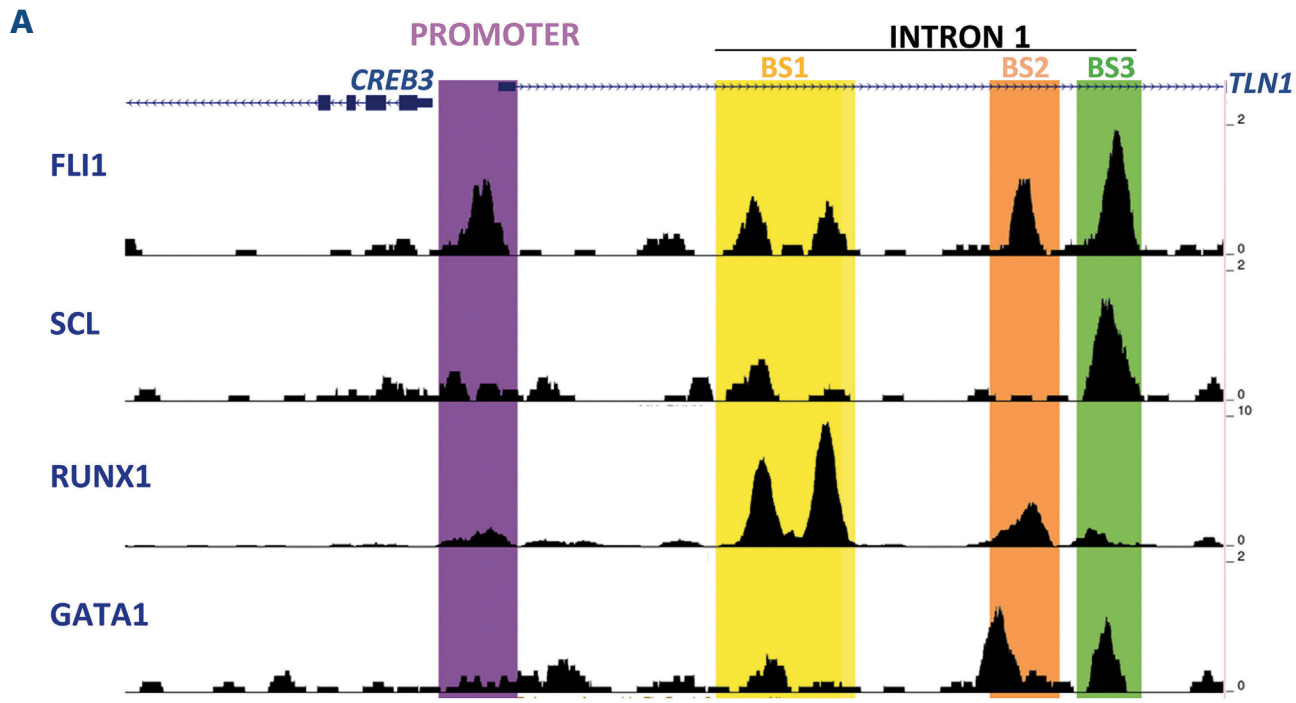

Figure 5. Identification and functional analysis of FLI1 regulatory regions in the *TLN1* gene. (A) Visualization of ChIP-seq peaks in the *TLN1* gene. FLI1, SCL, RUNX1 and GATA1 binding loci in the *TLN1* promoter region (purple) and intron 1 (yellow, orange, and green) are shown. BS: binding site. (B) Luciferase activity in HEL cells transfected with various pGL3 luciferase reporter vectors, including the empty vector (gray), the *TLN1* promoter (purple), or *TLN1* intron 1 regions (binding site 1 in yellow, binding site 2 in orange, and binding site 3 in green). The dual-luciferase assay involved sequential measurement of Firefly and Renilla luciferase activity in the same sample; results are presented as the ratio of Firefly to Renilla activity (Fluc/Rluc). The pGL3 vector lacking regulatory regions (empty vector) served as a normalization control. Each plasmid was assayed in three independent transfection experiments. **P*<0.05 *versus* pGL3-empty (Mann-Whitney test). (C) Luciferase activity in MSR cells transfected with empty luciferase reporter vector (pGL3 empty) or luciferase vector containing the intronic binding site 3 of *TLN1* (intronic BS3), along with the pCDNA-FLI1, pCDNA-GATA1, and pCDNA-SCL vectors as specified. The pCDNA empty vector (lacking transcription factors [TF]) served as a normalization control. Each plasmid was assayed in 3-6 separate transfection experiments. **P*<0.05, ***P*<0.01, ****P*<0.001 *versus* pCDNA-empty vector (Kruskal-Wallis test). $^{\#\#}$*P*<0.01 (Mann-Whitney test). (D) Luciferase activity in MSR cells transfected with intronic BS3 pGL3 luciferase reporter vector and pCDNA-GATA1 with WT FLI1 or FLI1 variants as indicated. Each plasmid was assayed in 2-5 separate transfection experiments. **P*<0.05 *versus* WT FLI1 + GATA1 (Mann-Whitney test).

complexes were observed for both conditions. Furthermore, when *TLN1* DNA was incubated with both protein extracts, a higher molecular weight complex was formed, thus indicating that when both proteins were present, they co-bound to the DNA. Accordingly, the amount of free DNA decreased as the higher molecular weight complex formed,

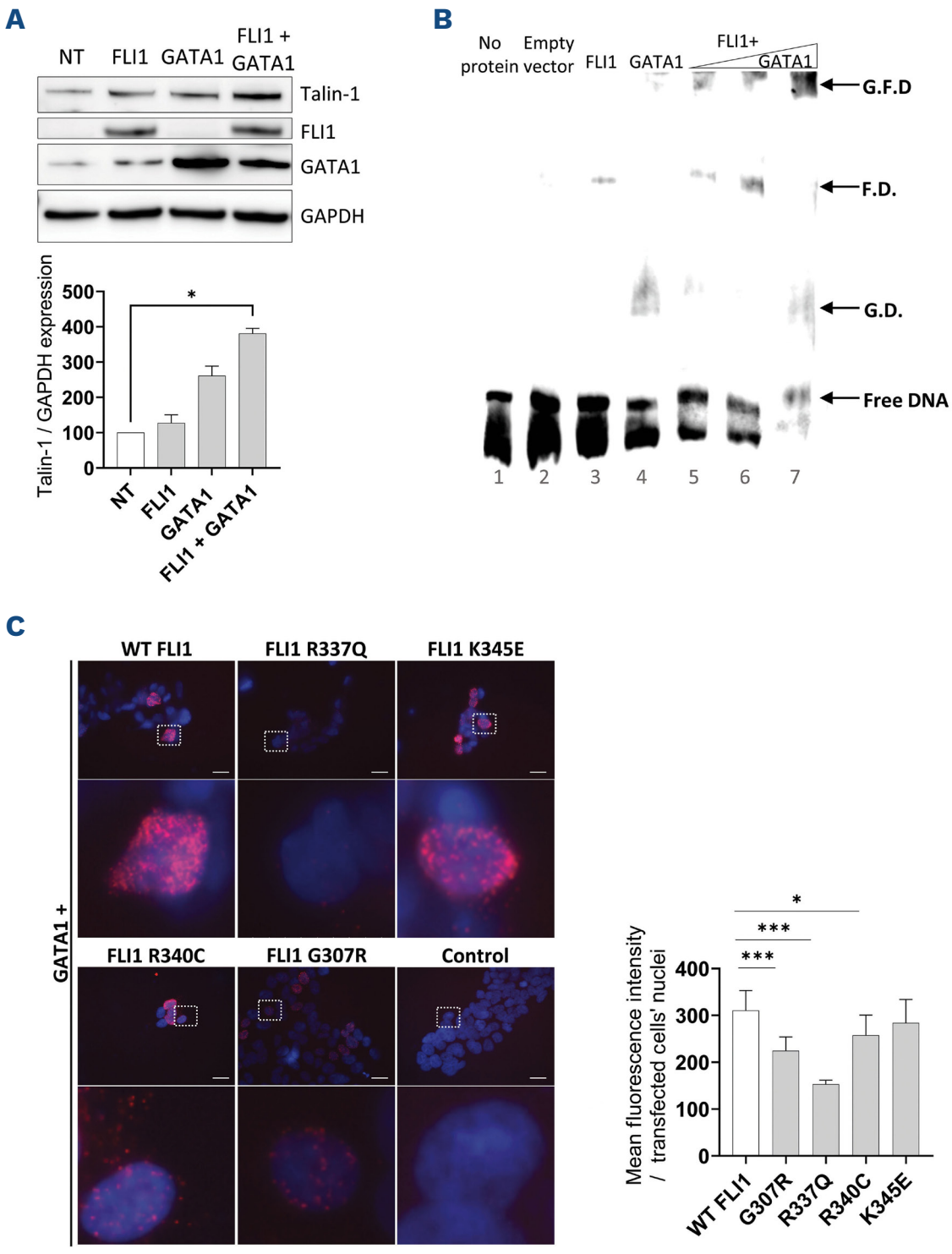

Figure 6. FLI1 and GATA1 cooperation and their interaction with *TLN1* intronic binding site 3. (A) Assessment of the impact of FLI1 and GATA1 overexpression on talin-1 protein levels. (Top) Western blot analysis of talin-1, FLI1 (anti-FLI1 antibody), and GATA1 (anti-GATA1 antibody), in MEG-01 lysates, either non-transduced (NT) or transduced with FLI1, GATA1 or both (14 days post transduction). GAPDH served as the loading control. (Bottom) Densitometric analysis results were normalized to GAPDH and are expressed as the mean ± standard error of the mean (SEM) of three independent experiments. **P*<0.05 *versus* NT (Kruskal-Wallis test). (B) EMSA assay performed with biotin-labeled *TLN1* intronic binding site 3 DNA probes and nuclear protein extracts from MSR cells transfected with either an empty vector, FLI1, or GATA1. Conditions 2 to 4 used 400 ng of nuclear extracts from cells transfected with the empty vector, FLI1, or GATA1, respectively. Conditions 5 to 7 used 400 ng of nuclear extracts from cells transfected with FLI1, combined with increasing amounts of nuclear extracts from cells transfected with GATA1 (120, 240, and 400 ng). Wedge symbol denotes those increasing GATA1 concentrations. No shift was observed in reactions without protein extract (condition 1) or with extracts from cells transfected with the empty vector (condition 2). A shift band was detected in reactions using extracts from FLI1-transfected (condition 3) or GATA1-transfected cells (condition 4), as indicated by the arrows. In reactions with extracts from cells transfected with both FLI1 and GATA1 (conditions 5 to 7), a higher molecular weight band shift was observed. (C) The physical interactions between WT FLI1 or FLI1 variants and GATA1 in MSR cells were assessed using a proximity ligation assay, as described in the Methods. Protein complexes of interest were visualized as red fluorescent dots, with DAPI-stained nuclei depicted in blue; scale bar, 5 µm. (Top row) Microscopy images at 40X magnification. (Bottom row) Zoomed-in view of a specific area of the top row images (indicated by a white dashed square). Quantification of the mean fluorescence intensity of red dots per transfected cell nucleus is shown at the bottom. **P*<0.05, ****P*<0.001 (Mann-Whitney test). FD: FLI1/DNA complexes; GD: GATA1/DNA complexes; GFD: FLI1, GATA1, and DNA complexes.

further reinforcing the evidence of interaction (Figure 6B). This observation corroborates our finding of several FLI1- and GATA1-binding motifs in the intronic binding site 3 sequence using the online Regulatory Sequence Analysis Tools (*data not shown*). We also examined the physical interaction between FLI1 (WT and variants) and GATA1 using a Duolink proximity ligation assay. The results showed that both WT FLI1 and the K345E variant interact with GATA1 in the nucleus, while the G307R, R337Q, and R340C FLI1 variants exhibited impaired interaction with GATA1 (Figure 6C).

Discussion

Pathogenic variations in the proto-oncogene *FLI1* have been linked to the dominantly or recessively inherited bleeding disorder, platelet type 21 (OMIM 617443).[7-9] In unrelated families, we discovered two novel FLI1 mutations and provided valuable phenotypic insights into this recently identified Mendelian disorder. We have previously suggested that the degree of protein dysfunction differs depending on the genetic variation.[9] Our findings suggest that various mechanisms contribute to the decrease in FLI1 activity, potentially explaining the varying levels of functional impairment. As a result, this leads to reduced expression levels of talin-1, a critical component in β3 integrin activation. The clinical symptoms observed in the carriers of the two new variants were characterized by cutaneous and mucosal bleeding. The oldest individual required RBC transfusions on several occasions. The valvular malformation in the child and history of interventricular communication in the adult patient required further investigation. Both Paris Trousseau and Jacobsen syndromes, which are caused by an 11q deletion affecting *FLI1* among numerous other genes, can involve heart malformations.[16,17] Indeed, the majority of 11q-patients have a congenital heart defect. Typically, congenital heart defects in Jacobsen syndrome are thought to be due to *ETS1* hemizygosity. *ETS1* is located close to *FLI1* and plays an important role in heart development. *ETS1*$^{-/-}$ mice display significant membranous ventricular septal heart defects at E15.5 to E17.5.[18] Several genes may be involved in the heart defect observed in patients with 11q deletion, with each gene playing a distinct role in the phenotype. As FLI1 is required to maintain endothelial cell identity, which is crucial for heart development,[19] FLI1 may also be involved in cardiac malformations. While the data from this study are not definitively conclusive, they suggest that all patients diagnosed with FLI1-related platelet disorders should undergo cardiac evaluation. Non-invasive diagnostic procedures, particularly cardiac and aortic ultrasounds, may detect asymptomatic cardiac defects. Early diagnosis may facilitate timely therapeutic interventions, such as the prevention of bacterial endocarditis or monitoring for aortic dilatation.

Platelet analysis of these cases suggested a diagnosis of storage pool disease, which aligns with findings from other studies.[7-9] Microscopy revealed large alpha granules in both patients. *MYH10*, which is typically suppressed during MK polyploidization,[20] was over-expressed in the patients' platelets, thus indicating a defect in the repressive transcriptional activity of FLI1 *in vivo*, as previously reported.[9] Overall, the clinical profiles of both patients with the novel FLI1 variations were consistent with *FLI1* gene dysfunction. The two new variants exhibited distinct characteristics. The R340C variant exhibited a loss of repressive activity *in vitro* and cytoplasmic sequestration (similar to the previously described variants K345E and R337Q), while the G307R variant displayed normal repressive activity *in vitro* and was able to reach the nucleus. These findings suggest that the G307R variant may retain the ability to enter the nucleus and bind to DNA. The analysis of the X-ray structure of FLI1 in complex with double-stranded DNA supports this hypothesis, as the residues R340 and K345 are located at the DNA/FLI1 interface and could potentially disrupt the DNA/FLI1 interaction. By contrast, G307 is located further away from the DNA/FLI1 interface and does not affect FLI1 binding to DNA. Nuclear accumulation of FLI1 is influenced by two distinct nuclear localization signals, nuclear localization signal 1 (at the N-terminal region, amino acids 62 to 126) and nuclear localization signal 2 (within the ETS domain, amino acids 277 to 360).[21] Mutagenesis experiments revealed the functional importance of five residues in the ETS domain of FLI1 (K325, K334, R337, R340 and K350), which may explain the nuclear import defect observed in the R337Q and R340C mutants. K345 has been shown to have a mild impact on nuclear import, thereby supporting our findings.[21] Additional mechanisms for the G307R and K345E variations were identified, potentially contributing to the observed phenotype. For example, we observed a 60% reduction in the half-life of the mutated protein. The role that homodimerization plays in the transcriptional activity of FLI1 remains unclear;[11] however, previous studies have suggested that homodimerization is significantly involved in the transcriptional activity of ETS transcription factor family members.[22,23] Analysis of the FLI1 homodimer structure revealed that R337, R340 and K345 do not participate in the homodimer interface, while G307 is located at the core of the homodimer interface and likely inhibits dimerization through steric hindrance.

Our study also aimed to identify the underlying pathological pathways for this bleeding disorder using scRNA-seq during hematopoiesis.

This study reveals an upregulation of several erythroid-related genes and the erythroid transcription factor KLF1 regulon, along with a downregulation of genes involved in megakaryopoiesis. This supports the previously described functional cross-antagonism between the transcription factors FLI1 and KLF1 in the control of erythroid *versus* megakaryocytic differentiation.[24–27]

This study also demonstrates the crucial role of FLI1 in the

regulation of *TLN1* expression. We found that platelet activation was the most dysregulated pathway, which aligns with the previous report implicating FLI1 in the transcription of several platelet genes, including *GP6, GPIBA, GP9, ITGA2B, MPL* and *MYH10*.[7,8,28-30] More recently, transcriptome analysis of platelets harboring a DNA-binding variant of FLI1 revealed an enrichment for gene annotations related to protein transport and found that SNX24 was down-regulated and was required for alpha granule biogenesis.[31] In our gene expression analysis, *GP1BA* and *GP9* were among the top 20 most down-regulated genes. Overall, this indicates that multiple aspects of platelet structure and function are compromised in the case of FLI1 dysfunction. We found that *TLN1* was significantly down-regulated. Talin-1 is a mechano-sensitive cytoskeleton protein that plays a central role in mechano-transduction in various tissues, such as the myocardium and blood vessels.[32] In genetic loss-of-function studies, talin-1 has been shown to be involved in the morphogenesis of heart valves.[33] Additionally, studies on zebrafish embryos carrying a *TLN1* variant have shown that a deficiency in talin-1 leads to abnormal cardiovascular morphogenesis and function, with reduced cardiac growth, ventricular shortening fraction, and heart rate.[34] Additional studies may help to determine whether FLI1 variants induce heart impairments through defective *TLN1* regulation. In platelets, talin-1 links the cytoskeleton to integrins $\alpha 2\beta 1$ and $\alpha IIb\beta 3$. Mice with selective disruption of talin-1 in MK exhibited platelets with impaired hemostatic function and spontaneous hemorrhaging.[35] In humans, talin-1 variations have never been associated with bleeding disorders, thus suggesting that germline variations that disrupt talin-1 function may be embryonic lethal, as observed in mice.[36] By analyzing the ChIP-seq of FLI1 in MK performed by the Göttgens laboratory,[15] four binding regions were identified in the *TLN1* gene. All binding sites were active in HEL cells. As these regions are co-occupied by FLI1, RUNX1, SCL and GATA1, we investigated potential cooperation. The FLI1-GATA1 cooperation synergistically enhanced *TLN1* transcription through binding site 3 in intron 1. This observation is consistent with earlier reports, which indicate that GATA1 binds to the FLI1 ETS domain through its zinc fingers, exhibiting significant DNA-binding cooperativity,[1] and characterized talin-1 deficiency in platelets from patients carrying a pathogenic variant of GATA1.[37] We observed a synergistic effect at the protein level in a MK-like cell line, which showed detectable levels of talin-1. Interestingly, the synergy between GATA1 and FLI1 was abolished in the case of all FLI1 mutations with the exception of the K345E mutant. The loss of synergy between GATA1 and FLI1 may provide insight into the pathogenicity of the mutated allele. The conserved synergy between K345E mutant and GATA1, despite reduced talin-1 levels in platelets from a patient carrying this variant, may be explained by the fact that the MSR model does not account for the protein instability of this variant. These findings underscore the importance of cooperation between transcription factors in the regulation of talin-1 and platelet function. Although our analysis focused on three transcription factors, other transcription factors may also be involved in *TLN1* transcription. This may explain why three of the analyzed regions lost activity in MSR cells, while activity remained in HEL cells, as MSR cells do not express most of the transcription factors involved in hematopoiesis.

In conclusion, this study describes 2 patients with novel FLI1 pathogenic variants, demonstrating distinct mechanisms. The study of these patients unraveled the key role of FLI1 in the regulation of *TLN1* transcription. Our findings suggest that talin-1 deficiency may contribute to the platelet dysfunction observed in patients with FLI1 variants.

Disclosure

No conflicts of interest to disclose.

Contributions

EG and MP designed and performed the experiments, and analyzed the data. EG, MP and MCA analyzed the data and wrote the manuscript. MVB, JS, EA and DB performed culture and functional experiments. LH, DP, JM, DPB and TB performed scRNA-seq analysis. JvA conducted the structural analysis experiments. MIK, CF, PS, PEM, the Hemostasis Unit of Lille, France (M. Daniel, C. Paris, A. Dupont, and A. Bauters) and AV performed clinical and biological characterization of patients. MP and MCA supervised the study.

Acknowledgments

The authors acknowledge the members of the Centre de Référence des Pathologies Plaquettaires (CRPP) for their contribution regarding clinical analyses as well as the patients and healthy donors. They also thank the high-performance computing center of Aix-Marseille Université for granting access to its high-performance computing resources, the Génomique et Genomique et Bioinformatique Marseille (GBiM) platform for the sequencing, and the Vect'UB platform (Bordeaux, France) for producing lentiviral particles.

Funding

The study was supported by the "Priority Research Program on Rare Diseases" of the French Investment for the Future Program (to MP: BIOFIT), the French Agency for Research (Agence Nationale de la Recherche – ANR; to MP: MOST) and by the National Institute of Health (to JvA: 5R01DK088327-10 and 5R01HL141366-04).

Data-sharing statement

To obtain raw data and protocols, please contact Elisa Gabinaud (elisa.gabinaud@univ-amu.fr) or the corresponding author Marjorie Poggi (marjorie.poggi@univ-amu.fr).

References

1. Eisbacher M, Holmes ML, Newton A, et al. Protein-protein interaction between Fli-1 and GATA-1 mediates synergistic expression of megakaryocyte-specific genes through cooperative DNA binding. Mol Cell Biol. 2003;23(10):3427-3441.
2. Huang H, Yu M, Akie TE, et al. Differentiation-dependent Interactions between RUNX-1 and FLI-1 during megakaryocyte development. Mol Cell Biol. 2009;29(15):4103-4115.
3. Bluteau D, Balduini A, Balayn N, et al. Thrombocytopenia-associated mutations in the ANKRD26 regulatory region induce MAPK hyperactivation. J Clin Invest. 2014;124(2):580-591.
4. Hart A, Melet F, Grossfeld P, et al. Fli-1 is required for murine vascular and megakaryocytic development and is hemizygously deleted in patients with thrombocytopenia. Immunity. 2000;13(2):167-177.
5. Moussa O, LaRue AC, Abangan RS, et al. Thrombocytopenia in mice lacking the carboxy-terminal regulatory domain of the Ets transcription factor Fli1. Mol Cell Biol. 2010;30(21):5194-5206.
6. Breton-Gorius J, Favier R, Guichard J, et al. A new congenital dysmegakaryopoietic thrombocytopenia (Paris-Trousseau) associated with giant platelet alpha-granules and chromosome 11 deletion at 11q23 [see comments]. Blood. 1995;85(7):1805-1814.
7. Stockley J, Morgan NV, Bem D, et al. Enrichment of FLI1 and RUNX1 mutations in families with excessive bleeding and platelet dense granule secretion defects. Blood. 2013;122(25):4090-4093.
8. Stevenson WS, Rabbolini DJ, Beutler L, et al. Paris-Trousseau thrombocytopenia is phenocopied by the autosomal recessive inheritance of a DNA-binding domain mutation in FLI1. Blood. 2015;126(17):2027-2030.
9. Saultier P, Vidal L, Canault M, et al. Macrothrombocytopenia and dense granule deficiency associated with FLI1 variants: ultrastructural and pathogenic features. Haematologica. 2017;102(6):1006-1016.
10. Bigot T, Gabinaud E, Hannouche L, et al. Single-cell analysis of megakaryopoiesis in peripheral CD34+ cells: insights into ETV6-related thrombocytopenia. J Thromb Haemost. 2023;21(9):2528-2544.
11. Hou C, Tsodikov OV. Structural basis for dimerization and DNA binding of transcription factor FLI1. Biochemistry. 2015;54(50):7365-7374.
12. Li G, Panday SK, Peng Y, Alexov E. SAMPDI-3D: predicting the effects of protein and DNA mutations on protein-DNA interactions. Bioinformatics. 2021;37(21):3760-3765.
13. Zhang N, Chen Y, Lu H, et al. MutaBind2: predicting the impacts of single and multiple mutations on protein-protein interactions. iScience. 2020;23(3):100939.
14. Herrmann C, Van de Sande B, Potier D, Aerts S. i-cisTarget: an integrative genomics method for the prediction of regulatory features and cis-regulatory modules. Nucleic Acids Res. 2012;40(15):e114.
15. Tijssen MR, Cvejic A, Joshi A, et al. Genome-wide analysis of simultaneous GATA1/2, RUNX1, FLI1, and SCL binding in megakaryocytes identifies hematopoietic regulators. Dev Cell. 2011;20(5):597-609.
16. Mattina T, Perrotta CS, Grossfeld P. Jacobsen syndrome. Orphanet J Rare Dis. 2009;4(1):9.
17. Krishnamurti L, Neglia JP, Nagarajan R, et al. Paris-Trousseau syndrome platelets in a child with Jacobsen's syndrome. Am J Hematol. 2001;66(4):295-299.
18. Ye M, Coldren C, Liang X, et al. Deletion of ETS-1, a gene in the Jacobsen syndrome critical region, causes ventricular septal defects and abnormal ventricular morphology in mice. Hum Mol Genet. 2010;19(4):648-656.
19. Weinstein N, Mendoza L, Álvarez-Buylla ER. A computational model of the endothelial to mesenchymal transition. Front Genet. 2020;11:40.
20. Lordier L, Bluteau D, Jalil A, et al. RUNX1-induced silencing of non-muscle myosin heavy chain IIB contributes to megakaryocyte polyploidization. Nat Commun. 2012;3(1):717.
21. Hu W, Philips AS, Kwok JC, Eisbacher M, Chong BH. Identification of nuclear import and export signals within Fli-1: roles of the nuclear import signals in Fli-1-dependent activation of megakaryocyte-specific promoters. Mol Cell Biol. 2005;25(8):3087-3108.
22. Lamber EP, Vanhille L, Textor LC, et al. Regulation of the transcription factor Ets-1 by DNA-mediated homo-dimerization. EMBO J. 2008;27(14):2006-2017.
23. Cooper CDO, Newman JA, Aitkenhead H, Allerston CK, Gileadi O. Structures of the Ets protein DNA-binding domains of transcription factors Etv1, Etv4, Etv5, and Fev. J Biol Chem. 2015;290(22):13692-13709.
24. Starck J, Cohet N, Gonnet C, et al. Functional cross-antagonism between transcription factors FLI-1 and EKLF. Mol Cell Biol. 2003;23(4):1390-1402.
25. Masuya M, Moussa O, Abe T, et al. Dysregulation of granulocyte, erythrocyte, and NK cell lineages in Fli-1 gene-targeted mice. Blood. 2005;105(1):95-102.
26. Buet D, Raslova H, Geay J-F, et al. p210BCR-ABL reprograms transformed and normal human megakaryocytic progenitor cells into erythroid cells and suppresses FLI-1 transcription. Leukemia. 2007;21(5):917-925.
27. Bouilloux F, Juban G, Cohet N, et al. EKLF restricts megakaryocytic differentiation at the benefit of erythrocytic differentiation. Blood. 2008;112(3):576-584.
28. Antony-Debré I, Bluteau D, Itzykson R, et al. MYH10 protein expression in platelets as a biomarker of RUNX1 and FLI1 alterations. Blood. 2012;120(13):2719-2722.
29. Deveaux S, Filipe A, Lemarchandel V, et al. Analysis of the thrombopoietin receptor (MPL) promoter implicates GATA and Ets proteins in the coregulation of megakaryocyte-specific genes. Blood. 1996;87(11):4678-4685.
30. Kwiatkowski BA, Bastian LS, Bauer TR, et al. The ets family member Tel binds to the Fli-1 oncoprotein and inhibits Its transcriptional activity. J Biol Chem. 1998;273(28):17525-17530.
31. Lacey J, Webster SJ, Heath PR, et al. Sorting nexin 24 is required for α-granule biogenesis and cargo delivery in megakaryocytes. Haematologica. 2022;107(8):1902-1913.
32. Wang Y, Huang H, Weng H, et al. Talin mechanotransduction in disease. Int J Biochem Cell Biol. 2024;166:106490.
33. Gunawan F, Gentile A, Fukuda R, et al. Focal adhesions are essential to drive zebrafish heart valve morphogenesis. J Cell Biol. 2019;218(3):1039-1054.
34. Wu Q, Zhang J, Koh W, et al. Talin1 is required for cardiac Z-disk stabilization and endothelial integrity in zebrafish. FASEB J. 2015;29(12):4989-5005.
35. Petrich BG, Marchese P, Ruggeri ZM, et al. Talin is required for integrin-mediated platelet function in hemostasis and thrombosis. J Exp Med. 2007;204(13):3103-3111.
36. Monkley SJ, Zhou XH, Kinston SJ, et al. Disruption of the talin gene arrests mouse development at the gastrulation stage. Dev Dyn. 2000;219(4):560-574.
37. White JG, Burris SM, Thomas A. Cytoskeletons of X-linked GATA-1, G208S macrothrombocytes are deficient in talin. Blood. 2008;112(11):1829-1829.